

Single-Domain Circular Nanomagnets

R. P. Cowburn,* D. K. Koltsov, A. O. Adeyeye, and M. E. Welland

Nanoscale Science Group, Department of Engineering, University of Cambridge, Trumpington Street, Cambridge CB2 1PZ, United Kingdom

D. M. Tricker

Department of Materials Science and Metallurgy, University of Cambridge, Pembroke Street, Cambridge CB2 3QZ, United Kingdom

(Received 15 January 1999)

The magnetic properties of deep submicron circular nanomagnets fabricated by high-resolution electron beam lithography from Supermalloy ($\text{Ni}_{80}\text{Fe}_{14}\text{Mo}_5$) have been studied as a function of both diameter (500–55 nm) and thickness (6–15 nm). A high sensitivity magneto-optical method has been used to measure the hysteresis loops of these nanomagnets. An experimental phase diagram in diameter and thickness has thus been produced which identifies a vortex phase and a single-domain phase. The two phases agree well with micromagnetic theory.

PACS numbers: 75.50.Tt, 75.30.Kz, 75.60.-d, 78.20.Ls

Magnetism at small length scales has in recent years provided a wealth of scientific interest and potential technological applications [1]. Recent advances in nanometer scale fabrication technology have opened up the possibility of studying artificially fabricated zero-dimensional magnetic systems in which all three dimensions are geometrically constrained on a nanometer length scale. These so-called nanomagnets form an excellent experimental laboratory for testing fundamental theorems in magnetostatics and micromagnetics [2]. Perhaps the most important of these theorems is Brown's fundamental theorem [3] which states that, because of a competition between magnetostatic energy and quantum mechanical exchange energy, magnetic domain formation should be entirely suppressed in very small ($\sim 10^{-8}$ m) magnetic particles, causing nanomagnets to behave as single giant spins. Experimental data on the bounds of validity of Brown's theorem in well-controlled systems are currently in great demand because "single-domain particles" are very promising candidates for high-density hard disk data storage and integrated magnetoelectronic devices such as nonvolatile magnetic memory [4].

In this Letter we present the results of a detailed study into the magnetic behavior of deep submicron circular nanomagnets fabricated by high-resolution electron beam lithography from the soft magnetic alloy Supermalloy as a function of both diameter (500–55 nm) and thickness (6–15 nm). We have fabricated small arrays comprising 10^2 – 10^3 identical particles and have measured the hysteresis loop (M - H loop) of the ensemble using a high sensitivity magneto-optical method. The high definition of the lithography means that all of the particles in the array are virtually identical to each other and so the measured *average* properties for the array can also be interpreted as the *individual* properties of a single nanomagnet. The shape of the hysteresis loops gives detailed information on

the magnetic state at remanence (i.e., under zero applied field) and on the mechanism by which the magnetization within each nanomagnet reverses under the action of an externally applied field. Using the hysteresis loops, we have been able to derive an experimental phase diagram of these properties as a function of nanomagnet diameter and thickness. We have been able to identify two distinct phases—a vortex phase and a single-domain phase—and to observe the transition between phases.

Two layers of polymethylmethacrylate, one of molecular weight 495×10^3 and one of weight 950×10^3 , were spun onto a single crystal silicon substrate. Arrays of circular disks were then exposed onto the sample in a JEOL 4000EX SEM/TEM, followed by 30 sec of development in a 1:3 solution of methyl isobutyl ketone/isopropyl alcohol. The array size was between $(5 \mu\text{m})^2$ and $(10 \mu\text{m})^2$; the spacing between each nanomagnet was always at least equal to the diameter of the nanomagnet, and for the smallest structures was as large as 3 times the diameter. This ensured that there was negligible magnetostatic interaction between nanomagnets. A 6–15 nm thick layer of $\text{Ni}_{80}\text{Fe}_{14}\text{Mo}_5$ ("Supermalloy") followed by a 5 nm thick antioxidation capping layer of gold was then deposited at a rate of 0.08 nm s^{-1} by electron beam evaporation in an ultrahigh vacuum chamber with base pressure 4×10^{-9} mbar. An unpatterned substrate was also present in the chamber to allow structural and magnetic characterization of the unpatterned magnetic film. Ultrasonic assisted lift-off in acetone was used to remove the magnetic film from the unexposed parts of the patterned sample.

Transmission electron microscopy (TEM) and cross sectional TEM showed the deposited Supermalloy to have a random polycrystalline microstructure with grains of size ~ 10 nm and a surface roughness of less than 0.5 nm. Scanning electron microscopy (SEM) was used to check the size and shape of the nanomagnets. Figure 1

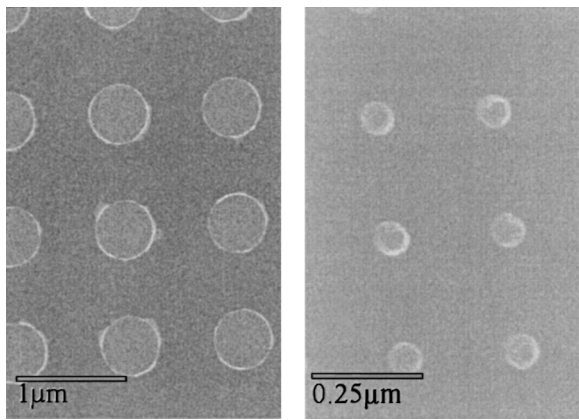


FIG. 1. SEM micrographs of circular nanomagnets of diameter 500 nm (left) and 55 nm (right).

shows some of these SEM images. These and other images showed that the distribution in diameter of the nanomagnets within an array was less than 2%.

In addition to this structural characterization, we have also performed magnetic characterization. Magneto-optical magnetometry was used to measure the coercivity (~ 1 Oe) and the anisotropy field (4 ± 1 Oe, uniaxial in plane) of the unpatterned film. A B - H loopier was used to check the thickness and saturation magnetization (800 ± 60 emu cm^{-3}) of the unpatterned film. Temperature dependent measurements showed the unpatterned films still to be ferromagnetic at 300°C , which is not inconsistent with the expected Curie temperature of 400°C and hence an exchange stiffness of $\sim 10^{-6}$ erg cm^{-1} .

We have obtained room temperature hysteresis loops from the arrays of nanomagnets using a high sensitivity magneto-optical method [5]. The sample surface can be viewed under an optical microscope while a laser spot (size $\sim 5 \mu\text{m}$) is moved over the surface until focused on top of one of the arrays of nanomagnets. The reflected laser beam is then polarization analyzed in order to access the longitudinal Kerr effect, which serves as a probe of the component of magnetization lying in the optical plane of incidence. An electromagnet allows magnetic fields of up to 1000 Oe to be applied in the plane of the sample.

Figure 2 shows the complete data set of measured hysteresis loops as a function of the diameter and thickness of the nanomagnets, normalized in height to remove the effects of thickness, array size, and array filling factor. The magnetic field was applied in the plane of the nanomagnets, in the direction of the uniaxial anisotropy easy axis. One sees from Fig. 2 two classes of loop, which are shown in detail in Fig. 3 with schematic annotation. The first is typified by the 300 nm, 10 nm loop [Fig. 3(a)]: As the applied field is reduced from minus saturation, the nanomagnets retain full moment, until a critical field slightly below zero, at which point nearly all magnetization is lost. The magnetization then progressively reappears as the field is increased from zero, until positive

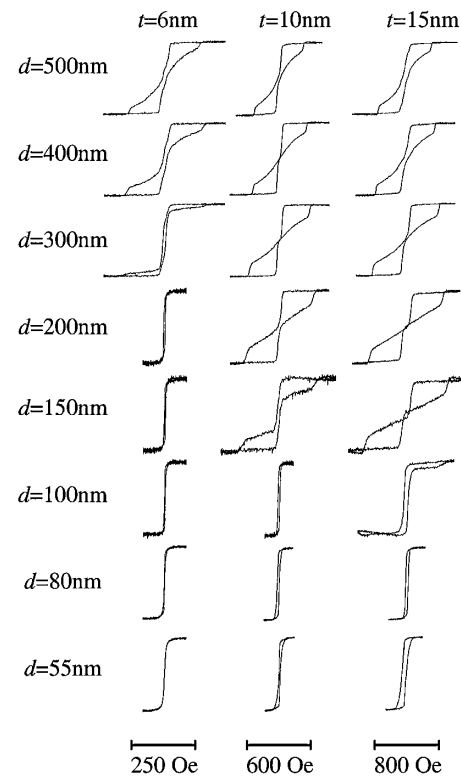


FIG. 2. Hysteresis loops measured as a function of diameter (d) and thickness (t) from circular nanomagnets. For each loop the horizontal axis is applied field and the vertical axis is magnetization.

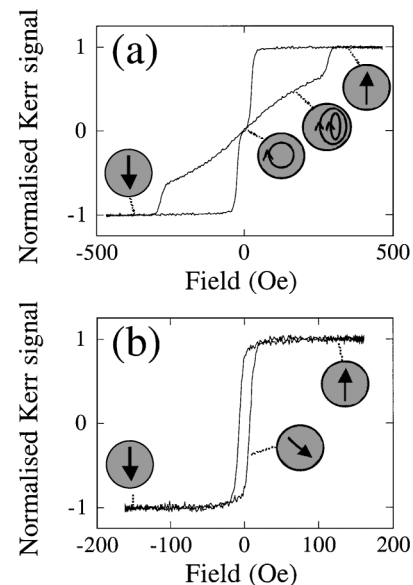


FIG. 3. Hysteresis loops measured from nanomagnets of diameter (d) and thickness (t): (a) $d = 300$ nm, $t = 10$ nm; (b) $d = 100$ nm, $t = 10$ nm. The schematic annotation shows the magnetization within a circular nanomagnet, assuming a field oriented up the page.

saturation is achieved. The sudden loss of magnetization close to zero field is very characteristic of the formation of a flux closing configuration; the simplest of these is a vortex in which the magnetization vector remains parallel to the nearest edge at all points in the circular nanomagnet. In large structures, this state lowers the system energy by reducing stray fields and hence lowering magnetostatic energy. Increasing the field then deforms the vortex by pushing its core away from the center of the nanomagnet, until it becomes unstable and the vortex is eventually annihilated [6], although not until a field of several hundred Oe has been reached.

The second class of loop is typified by the 100 nm, 10 nm loop [Fig. 3(b)]. These loops retain a high remanence ($\sim 80\%$) and switch at a very low field (~ 5 Oe). This is characteristic of single-domain behavior: All of the nanomagnets within the array retain all of their magnetization to form an array of giant spins, and magnetization reversal occurs by each giant spin rotating coherently [7]. In an earlier study [8] into the properties of *square* nanomagnets we found that the geometric shape of the nanomagnet imposed a strong magnetic anisotropy (called configurational anisotropy) which led to high reversal fields. The circular symmetry of the nanomagnets reported in this Letter means, however, that all in-plane magnetization directions are geometrically identical and so there is no configurational anisotropy. The only remaining anisotropy opposing the coherent rotation is then the weak in-plane anisotropy intrinsic to the Permalloy family. Hysteresis loops of this class thus have a saturation field of merely a few Oe's. We found that the remanence vanished if the field was applied parallel to the uniaxial hard axis instead of the easy axis, as would be expected for such a reversal mechanism.

In order to verify that the class of behavior typified by Fig. 3(a) is indeed due to vortex formation we have performed an *ab initio* numerical calculation [9] to simulate one-half of the loop. We have used the semiclassical formalism of micromagnetics [2] in which a numerical finite element method is used to find the magnetization vector field which minimizes a Hamiltonian incorporating magnetostatic energy and exchange energy terms. This calculation can be repeated at many different applied field values in order to simulate a complete hysteresis loop. We have used 5656 cubic finite element cells, each of length 5 nm and values of 800 emu cm^{-3} for the saturation magnetization (as measured experimentally from our continuous films—see above in this Letter), $1.05 \times 10^{-6} \text{ erg cm}^{-1}$ for the exchange stiffness (following Ref. [10]) and 4 Oe for the in-plane uniaxial anisotropy field (as measured from our continuous films, although this anisotropy is unimportant in the vortex phase).

Figure 4 shows the half loop which we have calculated for a circular nanomagnet of diameter 300 nm and thickness 10 nm [i.e., the same size as that measured in

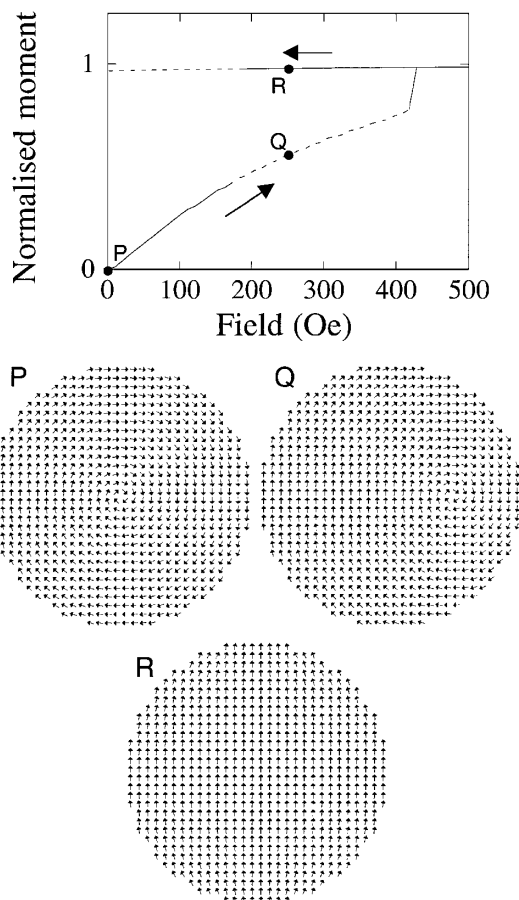


FIG. 4. A theoretically determined hysteresis half loop for a circular nanomagnet of diameter 300 nm and thickness 10 nm. The dashed parts of the loop indicate a metastable state. The calculated magnetization vector fields are shown for three points on the loop *P*, *Q*, and *R*, assuming a field oriented up the page.

Fig. 3(a)]. The precise mechanism by which a vortex is first nucleated is highly complex and is beyond the scope of this study. We therefore assume that a vortex is present under the zero field. One sees that as the applied field is increased from that point, the calculated loop traces out an almost identical path to that obtained experimentally in Fig. 3(a). Both show a small degree of curvature followed by an abrupt annihilation event at a field of several hundred Oe's. Figure 4 also shows the calculated magnetization vector fields within a single circular nanomagnet at three different points on the hysteresis loop. These agree well with the schematic representations shown in Fig. 3(a).

We have marked parts of the theoretical half loop of Fig. 4 by a dashed line. These correspond to metastable regions, i.e., those for which the magnetization configuration leads to a local minimum in the free energy but not a global minimum. Whether a thermally activated transition from the metastable state to the thermodynamic ground state is to occur depends upon the temperature and

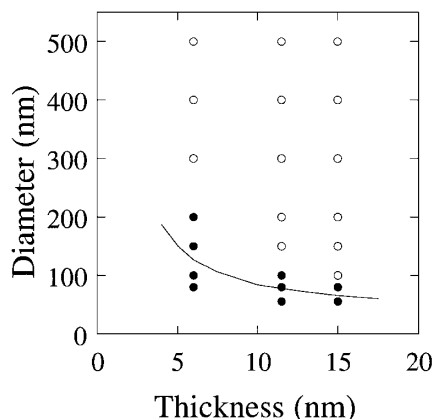


FIG. 5. An experimentally determined phase diagram. \circ = vortex; \bullet = single domain. The solid line shows a lower bound to the theoretical phase boundary between the vortex state (above the boundary) and the single-domain state (below the boundary).

the time scale over which the hysteresis loop is swept out. The theoretical simulation of Fig. 4 does not allow for thermally activated transitions, which accounts for the difference between the experimental and theoretical vortex annihilation fields of 283 and 423 Oe, respectively.

As the lateral size and thickness of the nanomagnets is decreased, our calculations show that the range of applied fields for which the vortex is metastable increases until the vortex can never nucleate and so the reversal mechanism must be replaced by the Stoner-Wohlfarth coherent rotation shown in Fig. 3(b). Figure 5 shows a phase diagram in nanomagnet size and thickness on which we show the calculated phase boundary below which vortex nucleation is impossible. We have also classified all of the experimentally obtained loops shown in Fig. 2 in terms of vortex or single-domain behavior and have plotted the result in Fig. 5. One sees that the experimental data agree very well with the theoretical line: No vortex nucleation was observed below it. We stress that the theoretical line is *not* a prediction for the transition from vortex to single-domain behavior, but is rather a lower limit to that boundary.

In conclusion, we have studied the magnetic properties of well-defined deep submicron circular nanomagnets made from Supermalloy. We have delineated an experimental phase diagram in diameter and thickness which identifies a vortex phase and a single-domain phase. In the vortex phase magnetization reversal proceeds by the nucleation and subsequent annihilation of a vortex under relatively strong fields. In the single-domain phase, reversal proceeds by a coherent rotation of the giant spin vector under very weak fields. The locations of these two phases on the phase diagram agree well with micromagnetic theory.

This work was supported by the Royal Society, St. John's College, Cambridge, and the U.K. EPSRC.

*Electronic address: rpc12@cus.cam.ac.uk

- [1] M. Hehn *et al.*, *Science* **272**, 1782 (1996); K.J. Kirk, J.N. Chapman, and C.D.W. Wilkinson, *Appl. Phys. Lett.* **71**, 539 (1997); C. Stamm *et al.*, *Science* **282**, 449 (1998); S. Wirth, M. Field, and D.D. Awschalom, *Phys. Rev. B* **57**, 14028 (1998); G. Meier *et al.*, *Appl. Phys. Lett.* **72**, 2168 (1998).
- [2] L. Landau and E. Lifschitz, *Physik. Z. Sowetunion* **8**, 153 (1935); W.F. Brown, *Micromagnetics* (Wiley, New York, 1963); A. Aharoni, *Introduction to the Theory of Ferromagnetism* (Oxford University Press, Oxford, 1996).
- [3] W.F. Brown, Jr., *J. Appl. Phys.* **39**, 993 (1968).
- [4] S.Y. Chou, *Proc. IEEE* **85**, 652 (1997); M. Johnson, *J. Vac. Sci. Technol. A* **16**, 1806 (1998); G.A. Prinz, *Science* **282**, 1660 (1998).
- [5] R.P. Cowburn, D.K. Koltsov, A.O. Adeyeye, and M.E. Welland, *Appl. Phys. Lett.* **73**, 3947 (1998).
- [6] R.E. Dunin-Borkowski, M.R. McCartney, B. Kardynal, and D.J. Smith, *J. Appl. Phys.* **84**, 374 (1998).
- [7] E.C. Stoner and E.P. Wohlfarth, *Philos. Trans. R. Soc. London A* **240**, 74 (1948).
- [8] R.P. Cowburn, A.O. Adeyeye, and M.E. Welland, *Phys. Rev. Lett.* **81**, 5414 (1998).
- [9] R.P. Cowburn and M.E. Welland, *Phys. Rev. B* **58**, 9217 (1998).
- [10] N. Smith, D. Markham, and D. LaTourette, *J. Appl. Phys.* **65**, 4362 (1989).